AIAA JOURNAL
Vol. 36, No. 12, December 1998

Interaction of Sound from Supersonic Jets with Nearby Structures

C. C. Fenno Jr.*
NASA Langley Research Center, Hampton, Virginia 23681-0001
A. Bayliss†
Northwestern University, Evanston, Illinois 60208
and
L. Maestrello‡
NASA Langley Research Center, Hampton, Virginia 23681-0001

We numerically solve a model of sound generated in an ideally expanded two-dimensional supersonic (Mach 2) jet. Two configurations are considered: 1) a free jet and 2) an installed jet with a nearby array of flexible aircraft type panels. In the later case the panels vibrate in response to loading by sound from the jet, and the full coupling between the panels and the jet is simulated, accounting for panel response and radiation as well as the jet acoustics. We consider the long time behavior of the jet/panel system and present results for the flowfield and far-field pressure and the vibration of, and radiation from, the panels. The pressure within the jet changes from a nearly discrete spectrum peaked at a preferred frequency f_*, which depends on properties of the jet, to a continuous spectrum as downstream distance increases. The far-field pressure is characterized by a highly directional beaming of sound with a spectral peak at f_* within the Mach line and a lower-level breakup into small-scale structures away from the Mach line. We show that the location of the panels relative to the Mach line is critical in determining panel response. Panels located upstream of the Mach line are subject to a low-level continuous spectrum loading and exhibit a comparable response. In contrast, panels located within the Mach line are subject to a high-level loading due to the intense Mach wave radiation of sound peaked at f_* and exhibit a comparable response. The panels radiate in a similar fashion to the sound in the jet. In particular, there is a strong beaming of sound waves at frequency f_* from the excited panels within the Mach angle from the bounding wall, indicating a significant effect of Mach wave radiation on both interior sound levels and spectral content in the supersonic regime.

Nomenclature

c_v = specific heat per unit volume
c_∞ = ambient sound speed
D = width of jet nozzle
E = total energy per unit volume, $\frac{1}{2}\rho(u^2 + v^2) + c_v\rho\tilde{T}$
f_* = preferred frequency of jet response
I = overall sound pressure level over time interval T, $(\int \tilde{p}^2\, dt/T)$, where the integral is taken over the time interval T
p = pressure
$\tilde{p}$ = $(p - p_0)/\epsilon$
Sr = Strouhal number based on jet exit velocity (fD/U_j)
Sr_* = Strouhal number at preferred frequency
T = interval in time over which solution is examined
$\tilde{T}$ = temperature
U_J = maximum jet exit velocity
u = x velocity
v = y velocity
x = horizontal coordinate
x_s = horizontal coordinate of source
y = vertical coordinate
y_j = vertical coordinate of jet centerline
ϵ = amplitude of the excitation source
ζ = vorticity, $(\tilde{v}_x - \tilde{u}_y)$
ρ = density
ω = circular frequency

Subscripts

x = derivative with respect to x
y = derivative with respect to y
0 = reference to local mean state
∞ = reference to ambient quantities

Superscripts

T = reference to transpose of a vector
$\tilde{}$ = difference between a quantity and its mean state divided by ϵ

Presented as Paper 97-0283 at the AIAA 35th Aerospace Sciences Meeting, Reno, NV, Jan. 6–9, 1997; received July 11, 1997; revision received June 14, 1998; accepted for publication July 10, 1998.

*National Research Council Resident Research Associate, Fluid Mechanics and Acoustic Division, MS 263; currently at Inter-National Research Institute, Newport News, VA 23602. Member AIAA.

†Professor, Department of Engineering Science and Applied Mathematics.

‡Senior Research Scientist, Fluids Mechanics and Acoustic Division, Mail Stop 463. Associate Fellow AIAA.

I. Introduction

In this paper we simulate the generation and propagation of sound in a supersonic jet 1) when the jet is free standing and 2) when the jet is installed near an array of flexible aircraft type panels. In both cases we consider a two-dimensional jet exiting from a converging-diverging (CD) nozzle extending to infinity in the upstream direction. In the installation case we employ a model in which the unsteady flowfield in the jet is fully coupled to the panel response and radiation. The jet is assumed to be ideally expanded in the steady state and to be at rest. In particular, for the installed jet we assume that the upstream state of the flowfield is the same on both sides of the panel array.

Aircraft panel vibration contributes to both structural fatigue of the panels and increased interior sound levels. An understanding of the jet/panel system is a necessary prerequisite to the control

of these effects. Our objectives in this paper are 1) to characterize sound generation mechanisms and propagation phenomena in an ideally expanded supersonic jet and 2) to characterize panel response and radiation under excitation by sound from the supersonic jet. The primary difference between the results presented here and previous results for subsonic jets[1–3] is the large-amplitude, highly directional Mach wave radiation associated with the supersonic jet. This results in an extreme location sensitivity in panel response, a highly directional sound field radiated from the panels, and a resulting significant variability in radiated sound levels and spectral content.

The jet is initially excited by a spatially and temporally localized source of transient mass injection of amplitude ϵ (Ref. 1). This leads to an initial acoustic disturbance that propagates through the jet. As a result of the excitation, instability waves are generated in the jet. These waves grow and then decay as they convect downstream, generating sound in the process. This phenomenon occurs over time scales much longer than that of the excitation pulse. The long time response of the jet is considered here and data are only presented after the wave due to the excitation pulse has exited the domain of interest. Thus, instability wave generated sound in the jet is simulated. The simulation does not directly account for sound generated by small-scale turbulent sources in the jet.

In previous work[1–3] we considered the jet acoustics, panel response, and radiation for subsonic jets. We showed that for low subsonic jets the acoustic response of the jet exhibited a nearly continuous spectrum and the panels acted as filters converting the broadband forcing into relatively narrow spectral bands. The effect of forward motion on low-speed jets was shown to reduce the level of the convective instability waves and thereby reduce the panel response and radiation. We further showed that, in contrast to the behavior for low subsonic jets, high subsonic jets exhibited a relatively peaked spectrum with a preferred peak frequency f_* that depended on the properties of the jet. The jet frequency f_* was present in the radiated pressure for a wide range of angles from the jet axis and thus in the pressure exciting the panels and the subsequent panel response and radiation.

The exact sources of jet sound have been identified from the basic equations of fluid dynamics.[4–9] However, these sources are generally not known in advance and must be modeled in some way for computation, e.g., to compute the loading on nearby panels. One way to enable modeling of the sources is to separate out the different effects that lead to sound generation in a jet. Convecting instability waves or large-scale structures act as sources of sound in a jet. This has been shown in experiments[10,11] and studied by analytical[12–15] and numerical[11,16,17] methods. In this paper sound generated from large-scale instability waves is computed. Small-scale turbulent structures are not considered. For supersonic jets it is known that the highest level of sound generated by instability waves convecting along the jet tends to propagate primarily at the Mach angle[18,19] and is thus referred to as Mach wave radiation. Supersonic jets operated under nonideal conditions also exhibit shock cell induced noise, an effect not considered here. In this paper only shock-free jets (at least in the steady state) are considered.

We employ a modified version of the Euler equations to calculate the long time response of the excited jet. In the jet flowfield this includes primarily convective instabilities propagating along the jet and generating pressure disturbances along the Mach line. As a result, the inviscid sources of jet sound are computed directly together with the resulting sound generation. The sound radiation from the jet serves to excite the panels, and we compute as well the panel response and radiation employing a self-consistent loading.

The computational domain is shown in Fig. 1. A modified version of the Euler equations is solved in two domains, the jet domain and the radiation domain, simulating the aircraft exterior and interior, respectively. These domains are separated by an array of six flexible panels joined to an infinite rigid wall at both ends. In addition to the fluid field in these two domains, panel response and radiation are also computed and are fully coupled to the fluid dynamics in the sense that at each time step the fluid dynamics (Euler) computation provides the pressure difference across the panels, thereby allowing computation of panel displacement and velocity. The resulting panel velocity then serves as a boundary condition for the

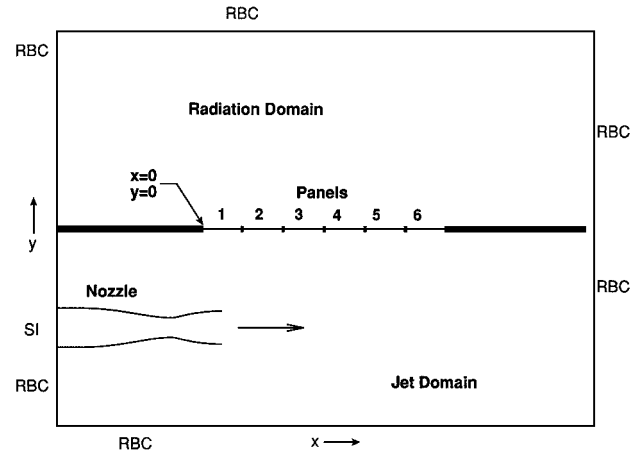

Fig. 1 Computational domain for installed jet, indicating the origin of coordinates and those boundary conditions where radiation boundary conditions (RBC) and supersonic inflow (SI) conditions are imposed. Note that the figure is not drawn to scale.

Euler computation. Thus, the panel excitation is obtained in a self-consistent manner directly from the Euler computation rather than from extrinsic phenomenological models. Similar computations for boundary layers and for panels excited by large-amplitude acoustic disturbances in an ambient medium have also been performed.[20,21]

In Sec. II we describe the model and the resulting numerical method. In Sec. III we present our results. We summarize our conclusions in Sec. IV.

II. Model and Numerical Method

Referring to Fig. 1, unsteady pressure, density, and velocity are computed in both the jet and radiation domains. In the jet domain, the jet, exiting from a CD nozzle of width D, is excited by a spatially and temporally localized source of mass injection. This leads to the generation of a train of instability waves that propagate along the jet, decaying beyond the potential core of the jet and generating sound. The sound serves to excite the panels, leading to both panel vibration and sound radiation into the jet and radiation domains, i.e., for a real aircraft into both the exterior and interior. For our two-dimensional model, it is difficult to identify panel radiation in the jet domain, as the panel radiation is small or at most of the same order of the sound generated within the jet. However, in the radiation domain the only source of sound is from panel vibration.

The wall boundary between the two domains consists of six flexible panels as indicated in Fig. 1. The panels are rigidly clamped to stringers separating any two adjacent panels and the wall is assumed to extend rigidly to infinity in both directions beyond the panels. The panels will be referred to as panels 1–6, numbered in ascending order as the downstream distance increases.

The computation of the nonlinear beam equation governing the panel responses is fully coupled to the Euler computations performed in both the jet and radiation domains. At each time step the pressure difference across the panels, obtained from the Euler computations, serves as a forcing term for the beam equation. The displacement obtained from the beam equation is differentiated in time and is then employed as a boundary condition on the normal velocity for the Euler computation. In the Euler computations the deflection of each panel is assumed to be small relative to the Euler length scales and so the Euler boundary is treated as a horizontal line. The Euler computations employ a (2–4) version of the MacCormack scheme.[22] Second-order finite differences combined with semi-implicit time differencing are used to solve the beam equation for each panel. The computation for the panels is performed on a different grid than the Euler grid, with interpolation used to transfer data between the two grids. Further details on both the coupling and the numerical scheme are given in Refs. 1–3.

The Euler equations are solved in conservation form for the vector $\hat{w} = (\rho, \rho u, \rho v, E)^T$. The pressure p is obtained from the equation of state. The Euler equations are modified in the jet domain to account for the jet flow. The jet exits from a nozzle of width D,

and the solution is computed both within and exterior to the nozzle. The Euler equations are modified to account for two different nonhomogeneous forcing terms.[3] One term serves as an excitation pulse to excite the jet. It corresponds to a localized source of mass injection at the location (x_s, y_j), where $x_s = 1.15D$. An alternative approach involves time harmonic excitation of the jet through boundary conditions.[23] The second forcing term is designed so that in the absence of the starter pulse the solution to the Euler equations would be a stationary profile corresponding to a spreading jet. Mean profiles for u_0, v_0, ρ_0, and $\tilde{T}_0$ are employed and are described in more detail elsewhere.[3] The inclusion of this term separates the computation of disturbances, in particular the resulting instability waves, from the computation of the mean flow, i.e., the spreading jet. Thus, the resulting system of equations allows for the simulation of instability waves and the resulting sound generation, together with the propagation of acoustic waves in the jet flowfield, without requiring the computation of the spreading jet itself. Although this is a simplified model, it captures many of the observed features of instability wave generated jet sound and permits high-resolution computation of the coupling of jet sound with the flexible panels and the resulting radiation from the panels. In particular, the model allows for computation of the natural sources of jet sound (the instability waves) together with the sound radiated by these sources.

Radiation boundary conditions are employed on all exterior boundaries except for the nozzle inflow where characteristic boundary conditions are employed. We employ an adaptive procedure in which the parameters in the boundary operator are varied so as to minimize a measure of the error of the boundary condition. These are described in detail elsewhere.[1-3]

III. Results

The computation includes both the near-field (including jet flow convective instabilities and large-scale structures) and far-field acoustic jet response, unsteady disturbances in the nozzle, the responses of each of the panels to excitation from jet disturbances, and radiation from the vibrating panels. The long time behavior of disturbances is considered to distinguish intrinsic properties of the jet from the frequency spectrum of the excitation pulse (the results do depend on the amplitude of the excitation pulse). Results are presented for two computations, one for a free jet and one for an installed jet located approximately $7D$ from the wall. For the installed jet, the panels were of length $3.5D$ (the other parameters were typical of aluminum). The frequencies were such that the wavelengths of the pressure just below the panels were of the same order or larger than the panel length. We note that a computation with shorter panels relative to D, so that the wavelengths were small compared with the panel length, could give very different results. In each case the computational domain extends $90D$ downstream from the nozzle exit and $60D$ upstream. In the free jet computation the domain extends $30D$ from the jet in both the positive and negative y directions. For the installed jet computation, the vertical range extends $60D$ from the wall in each direction. All results presented are for a jet with an exit Mach number of 2.0. For this Mach number the Mach angle is 30 deg. For all runs presented here we took $\epsilon = 5$.

We have extensively examined the accuracy of the numerical computations. The accuracy depends on both the location of the point in space and the time interval over which the solution is computed. The accuracy will degrade as the time interval of the computation increases. Furthermore, points closer to the artificial boundaries will be more affected by spurious boundary reflections. The data presented here have been validated by both grid refinements and boundary refinements (i.e., comparing the solutions obtained with different locations of the artificial boundaries) to be graphically accurate, i.e., within 10% pointwise error. Indeed, for each case presented here, the points and time intervals selected were chosen so as to maintain the graphical accuracy. In particular, the solution is only presented in a region bounded away from the boundaries. In addition, every effort has been made to consider the long time response of the jet, i.e., to not include the excitation pulse and, in the case of the installed jet, the primary reflection of the excitation pulse from the wall. Thus, the time intervals of the data at any particular point were chosen to reflect both accuracy and long time behavior.

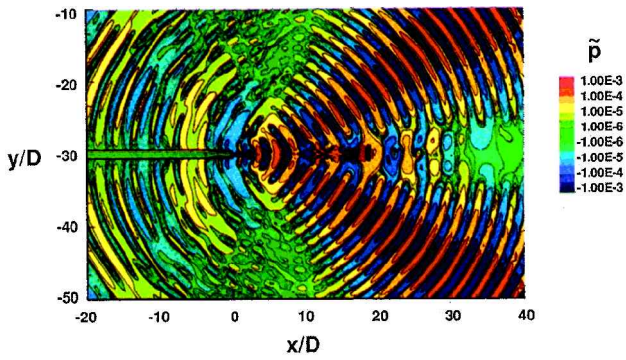

Fig. 2 Contours for $\tilde{p}$ for free jet.

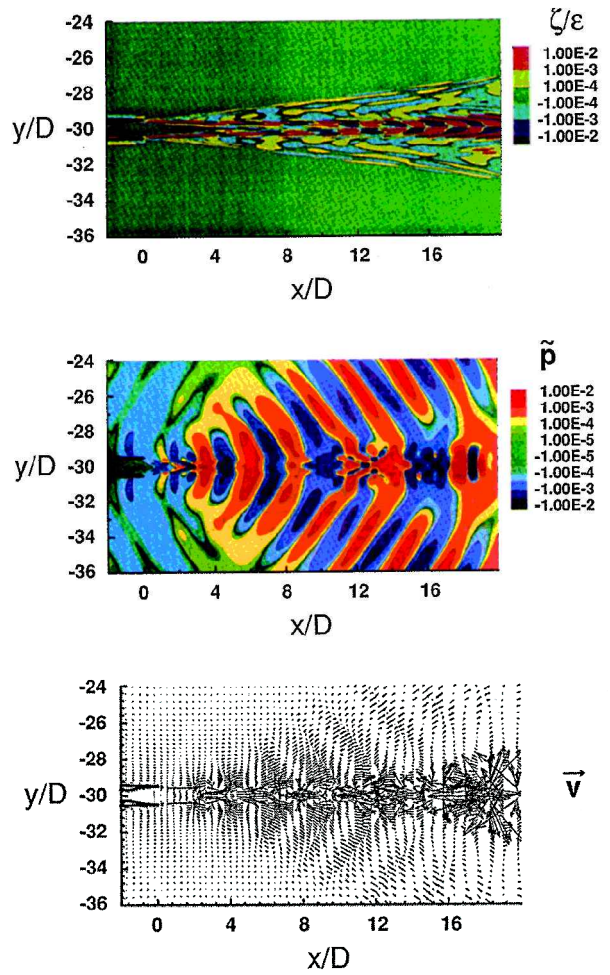

Fig. 3 Contours for vorticity (upper panel), $\tilde{p}$ (middle panel), and unsteady velocity field (lower panel) for region near nozzle exit for free jet.

A. Free Jet

In this case the upper and lower boundaries are artificial and the free jet is located in the center of the computational domain $(y/D = -30)$ so as to minimize boundary reflections. Figure 2 shows contours of scaled unsteady pressure $\tilde{p} = (p - p_0)/\epsilon$ at a fixed instant of time $(tc_\infty/D = 100)$, where p_0 is the local pressure in the steady (mean) flow, long after the excitation pulse has decayed and the initial acoustic wave generated by the pulse has passed out of the computational domain. The region between the contour lines is shaded according to the contour levels. Figure 2 shows a clear and well-defined beam of relatively large values of $|\tilde{p}|$ (on the order of 10^{-3}) centered at approximately 30 deg from the jet axis, the Mach angle for this jet. The relatively constant spacing between the outgoing waves suggests a highly peaked spectrum, which is indeed

the case, as will be seen later. Upstream of the Mach line, the radiation is much weaker, as indicated by the contour shading, and exhibits a more continuous spectrum, as indicated by the lack of a regular spacing between contours. Furthermore, there is a breakup into small-scale structures indicating a preferred upstream radiation for high frequencies. In the jet there is a train of large-scale pressure disturbances, generated at the nozzle lip and locally unstable, which propagate along the jet. This figure, although at a fixed instant of time, is typical of the behavior exhibited by $\tilde{p}$ after the excitation pulse has decayed. The highly localized beam of intense radiation is a manifestation of Mach wave radiation generated by the expansion and contraction of disturbances near the nozzle lip forming a cellular structure in the jet. As these cells expand and contract through one cycle, they generate Mach wave radiation propagating into the far field at the Mach angle of the flow with respect to the jet axis. The relatively peaked spectrum Mach wave radiation is superimposed on a low-level, nearly continuous spectrum, radiation pattern.

Comparison of Fig. 2 and the analogous figure presented in Ref. 3 for a high subsonic jet indicates the effect of a supersonic jet velocity on the resulting acoustic field. The acoustic field in Fig. 2 is highly directional in character, beamed in the direction of the Mach line. Furthermore, it is only within this localized beam that a clear peak frequency (characterized by a regular spacing between contours) is apparent. This beam represents Mach wave radiation. Outside of this beam, the acoustic pattern breaks up into smaller-scale disturbances at a much lower level with no peak frequency visible. In contrast, for high subsonic jets[3] the peak frequency is visible at all angles outside of a small region near the jet axis. There is a peak in the far-field directivity pattern at mid angles (this is characteristic of lower jet velocities as well), but it is much less pronounced than in the supersonic case. Both the supersonic and the subsonic jet exhibit sound radiation from instability waves in the jet. In addition to this generation effect, supersonic jets exhibit a propagation effect whereby acoustic energy is primarily carried along characteristics within the Mach line. This accounts for the pronounced beaming observed in the figure.

Figure 3 shows contours of vorticity ζ and $\tilde{p}$ (upper two panels, respectively) and the direction field for the unsteady velocity (lower panel) for a small region near the nozzle exit. The vorticity figure shows a train of vortices propagating along the jet axis and also along the jet boundary. Detailed examination shows that these vortices are generated at the nozzle lip. The vortices have a stretched appearance. Detailed comparison with lower-Mach-number jets shows that the stretching increases significantly with Mach number. The pressure contours (middle panel in Fig. 3) show a sequence of pressure disturbances associated with the vorticity disturbances. These disturbances, together with the velocity disturbances shown in the bottom figure, give rise to a cellular structure within the jet. These cells compress and expand in a nearly periodic fashion, generating Mach wave radiation propagating into the far field at the Mach angle with respect to the jet axis. The Mach wave radiation is indicated by the alternating light and dark structures propagating away from the jet axis. The cellular structure of the pressure correlates with the cellular structure in the velocity field shown in the bottommost panel. The Mach wave radiation is generated via cycles of contraction and expansion of the cells as they propagate downstream. We also note the incipient formation of the characteristic diamond-shaped cell. The downstream part of the diamond from a supersonically established flow whose origin is inside the nozzle is clearly visible at the nozzle exit.

Figure 4 shows the near-field $\tilde{p}$ in both the time and frequency domains. The data are taken along the horizontal line $(y - y_j)/D = 0.4$

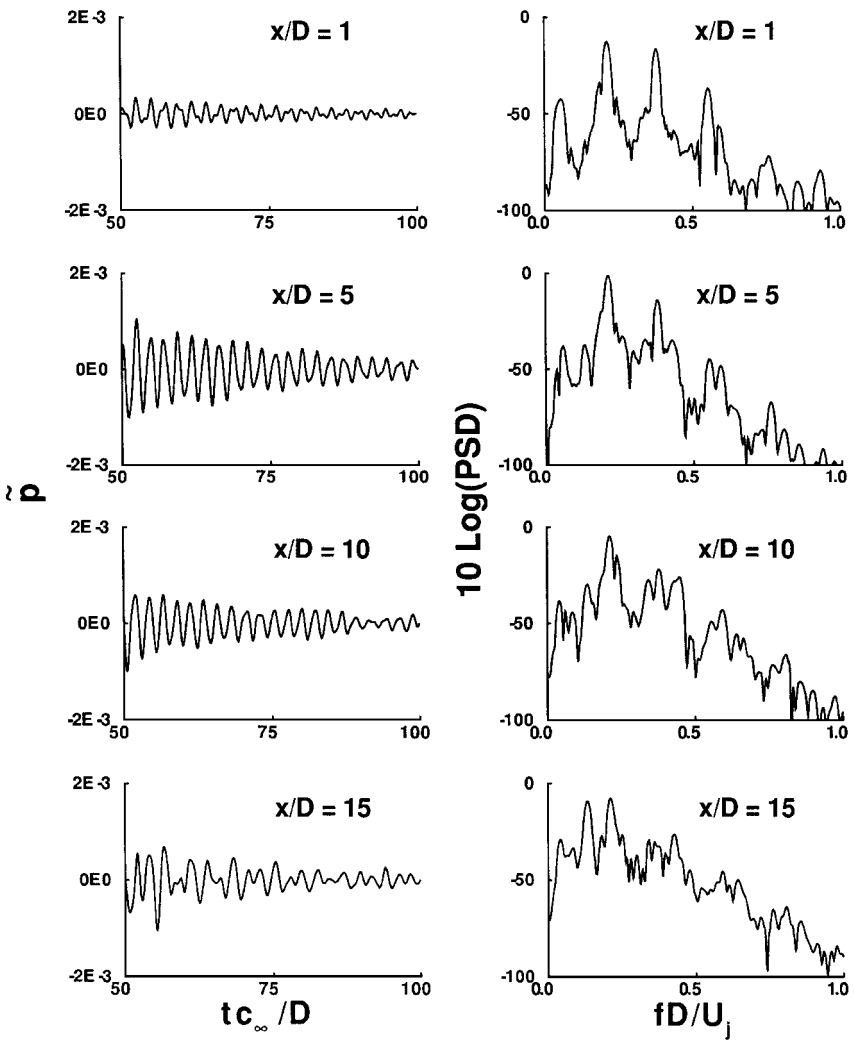

Fig. 4 Near-field $\tilde{p}$ in both time and frequency domains for free jet.

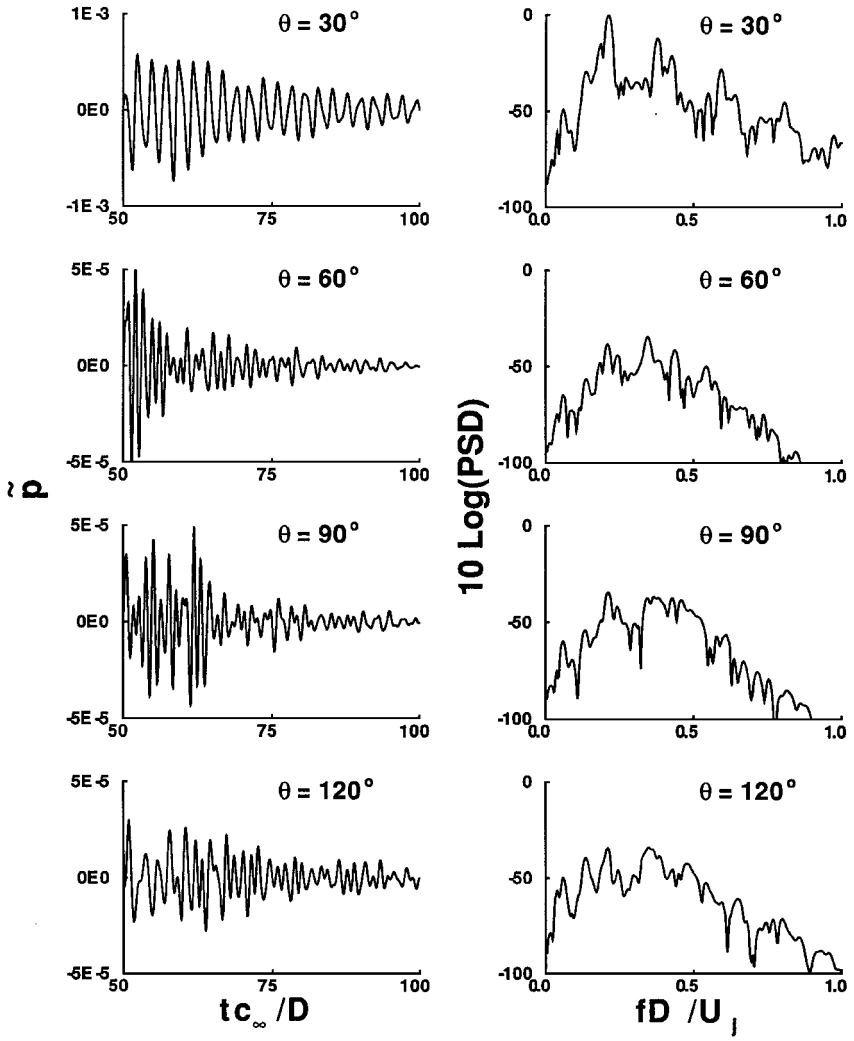

Fig. 5 Far-field $\tilde{p}$ in both time and frequency domains for free jet.

where $y_j = 30D$ for the free jet. Thus the data are taken on a horizontal line just below the vertical coordinate of the nozzle lip. The data are presented at four different axial locations in both the time and frequency domain. For the frequency domain data we compute the power spectral density (PSD) for $\tilde{p}$ by first Fourier transforming $\tilde{p}$ to obtain $\tilde{p}(\omega)$ and then computing the square of the amplitude $|\tilde{p}(\omega)|^2$. In Fig. 4 as well as in similar figures, we normalize the PSD by the maximum of the spectral data for all of the graphs in the figure. Thus the amplitudes of the PSDs for all graphs within each figure are commonly normalized.

The first point, $x/D = 1$, is in the vicinity of the interface between the potential flow core and the shear layer. All other points shown are well outside of the potential flow core of the jet. The spectral data, which in Fig. 4, as well as in other similar figures, are taken from the same time interval as shown in the time plots, are plotted against Strouhal number $Sr = fD/U_j$. Note that only the long time data are plotted and spectrally analyzed and that the initial transient has been excluded from the figure. Also note that the solution appears to be decaying slowly in time, indicating that, due to the convective nature of the jet disturbances, without further excitation all disturbances will eventually decay.

The data at $x/D = 1$ are small relative to the other x locations and exhibit well-defined spectral peaks. The second peak is at the peak Strouhal number of the Mach wave radiation ($Sr_* \simeq 0.21$). This Strouhal number and associated frequency f_* will be referred to as the jet Strouhal number or frequency and is close to the peak frequency observed in experiments for jets in this Mach number range.[19] The data for $x/D = 5$ exhibit strong spectral peaks in a band centered at Sr_* and another band near its harmonic. The last two downstream locations ($x/D = 10$ and 15) indicate the development of a more continuous spectrum, particularly in the low frequencies, as the downstream distance increases. The spectrum for $x/D = 15$ represents the spectrum of the large-scale structures in the jet that propagate and eventually decay beyond the potential core (refer to Fig. 2). Note that from Fig. 2 very little sound is generated beyond $10D$.

The far-field $\tilde{p}$ is shown in Fig. 5, with data taken on a circle of radius $30D$ centered on the source location (very near the nozzle exit). The data show peak radiation for angles near 30 deg consistent with Fig. 2 (observe that the time trace for 30 deg is plotted using a different scale than for the other angles). The spectra are again normalized so that the maximum of all four spectra in the figure corresponds to 0 db. The transition from the well-defined spectral peaks at the Mach angle 30 deg to a smaller, nearly continuous spectrum as the angle increases, i.e., for 60 deg and beyond, is an indication of the directivity of the Mach wave radiation for supersonic jets and is in contrast to the directivity found for all angles away from the jet axis for high subsonic jets.[3] Experiments with low-Reynolds-number jets indicate a very peaked spectrum for the Mach wave radiation.[19,24] Higher-Reynolds-number jets exhibit a somewhat more continuous spectrum, possibly due to the effect of small-scale turbulent fluctuations that are not accounted for in the present model. There is also a significant broadening of the spectrum towards higher frequencies as the angle increases, i.e., as the far-field location becomes more upstream.

Finally, in Fig. 6, the overall sound pressure level, $10 \log I$, plotted as a function of far-field angle, is examined. The figure shows a strong peak near 30 deg, consistent with many experimental measurements, together with a smaller peak upstream (angles near 150 deg) similar to the peak sometimes observed for jets in this Mach number range.[19] This peak is deemphasized by the presence of the wall (see the following).

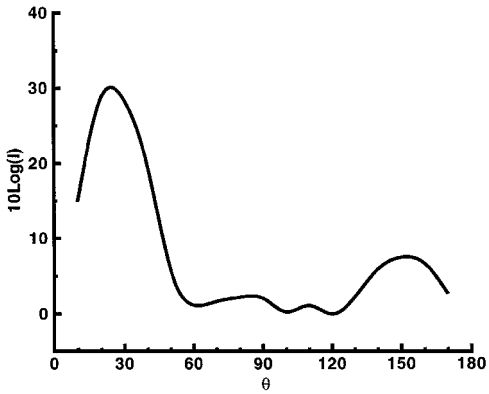

Fig. 6 Far-field directivity for free jet.

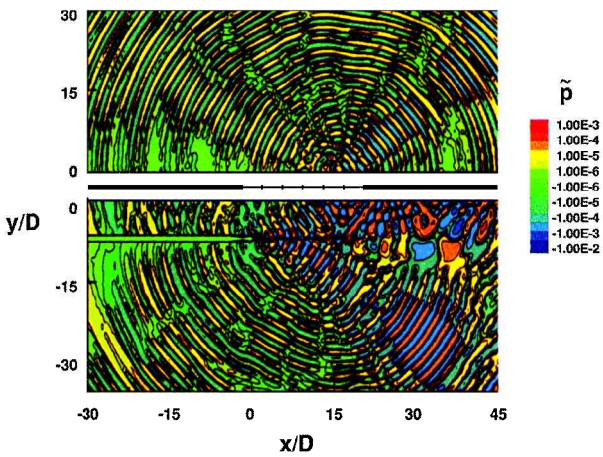

Fig. 7 Contours for $\tilde{p}$ for installed jet. Both jet domain (lower panel) and radiation domain (upper panel) are shown.

B. Jet and Flexible Wall Interaction

We next consider the installed jet. In Fig. 7 contours of $\tilde{p}$ are shown for both the jet and radiation domain at a fixed instant of time ($tc_\infty/D = 100$, the same nondimensional time as for Fig. 2). We note that at this late time there have been multiple reflections and interactions between the jet pressure and the wall so that significant differences in pressure contours between Figs. 7 and 2 are to be expected even close to the nozzle exit. The placement of the panels relative to the nozzle exit is as indicated in Fig. 7. The Mach wave radiation below the panels, similar to that for the free jet, can be seen in the lower part of Fig. 7. The Mach wave radiation is less regular than for the free jet, indicating a significant effect of reflections from the wall on the directivity and spectral content in the jet domain. The jet wall interaction includes both reflections from the wall as well as radiation from the panels. Generally, the panel radiation is small compared with wall reflections. Because the predominant signal impinging on the panels is in the vicinity of the Mach line, panels upstream of the Mach line have less influence in both reflection and radiation than the more downstream panels. Figure 8 shows the jet domain far-field directivity taken at points below the jet axis, i.e., away from the wall. The results show a significant deemphasis of the peak at 150 deg induced by the presence of the wall. There are also large pressure disturbances near the wall in the jet domain. Detailed examination shows that these disturbances convect downstream. We note that for both Figs. 8 and 6 the I is scaled so that the 0-db level occurs at the minimum of each of the figures.

Many of the directivity features in the jet domain are transmitted to the radiation domain. The most pronounced feature is a beaming from the panels at approximately 30 deg into the radiation domain. The spectrum of this radiation is peaked at f_* as it is for the Mach wave radiation in the jet domain. At larger angles, i.e., pointing more toward the upstream, the radiated pressure is dominated by smaller scales (higher frequencies), also similar to the jet domain. Note a zone of very low level radiation near 180 deg that may be below the accuracy of the computation.

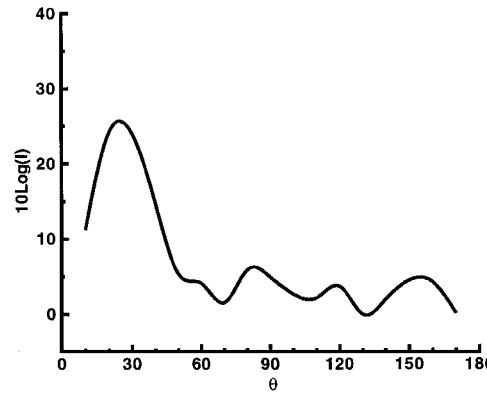

Fig. 8 Far-field directivity for installed jet.

We next consider panel response and radiation. In computing the responses of the panels, we endeavored to ensure that the response was due to the long time behavior of the jet rather than to the initial wave generated by the excitation pulse. This is more critical than for the free jet due to the low damping of the panels. The panels were kept rigid; i.e., the loading pressure—difference in pressure between the radiation and jet domains—was set to zero up to a certain time. This time was chosen so that the initial wave generated by the excitation pulse had passed away from the panels and could no longer serve to force the panels. The panels were then allowed to vibrate as the loading pressure was slowly increased to the true pressure difference. Thus the panel response does not include effects from the excitation pulse or from an abrupt switching on of the loading pressure.

The long time pressure just below the panels and at the panel centers is shown in Fig. 9 in both the time and frequency domains. Similarly, the velocity at each of the panel centers is shown in Fig. 10. Note that the scales for the time domain plots are not the same for each panel. In both figures the spectra are normalized to 0 db by the maximum for all of the panels. A significant change is seen in the character of $\tilde{p}$ as the panel location shifts downstream. For the most upstream panels (panels 1 and 2), $\tilde{p}$ is at a lower level and there are no well-defined spectral peaks. This is indicative of the breakup of the upstream radiation pattern into small-scale structures for the supersonic jet. As the downstream location increases, the spectra become increasingly peaked. The peak frequency corresponds to the jet frequency Strouhal number Sr_*. Note, for example, that for panels 4–6 the spectrum is dominated by Sr_* and its harmonic. Furthermore, the level of the forcing is nearly two orders of magnitude greater for the downstream panels than for the upstream panels. The results show that the Mach wave radiation results in an extreme sensitivity of the panel loading to the location of the panels. These conclusions are consistent with the panel response data shown in Fig. 10. The panel response increases by almost two orders of magnitude from panel 1 to panel 6, consistent with the increased loading due to the Mach wave. In addition, the spectral response becomes highly peaked for those panels that are excited by the Mach wave radiation in the jet domain.

We next consider the pressure in the radiation domain. The transmitted pressure, i.e., the pressure just above the panels, exhibits a behavior similar to that shown for v and is not shown. We consider instead the pressure along the line $y = 25D$ in the radiation domain. Figure 11 shows the radiated pressure at four different locations along this line. There is a large increase in level for points within the radiation beam (see the upper contour plot in Fig. 7). Note that the data are taken along a line, not a circle, and thus the increase in level with x occurs in spite of the radial decay that should reduce the radiated pressure for large values of x. Also note the emergence of a distinct peak near the jet frequency for points within the beam, e.g., the third graph in Fig. 11. This is also apparent in the fourth graph but is masked somewhat in view of the fact that less data are available over the given time interval due to the large value of x. These results suggest that for supersonic jets both the amplitude and frequency spectrum of the interior sound will be very sensitive to location, with the determining factor being the beam emanating at

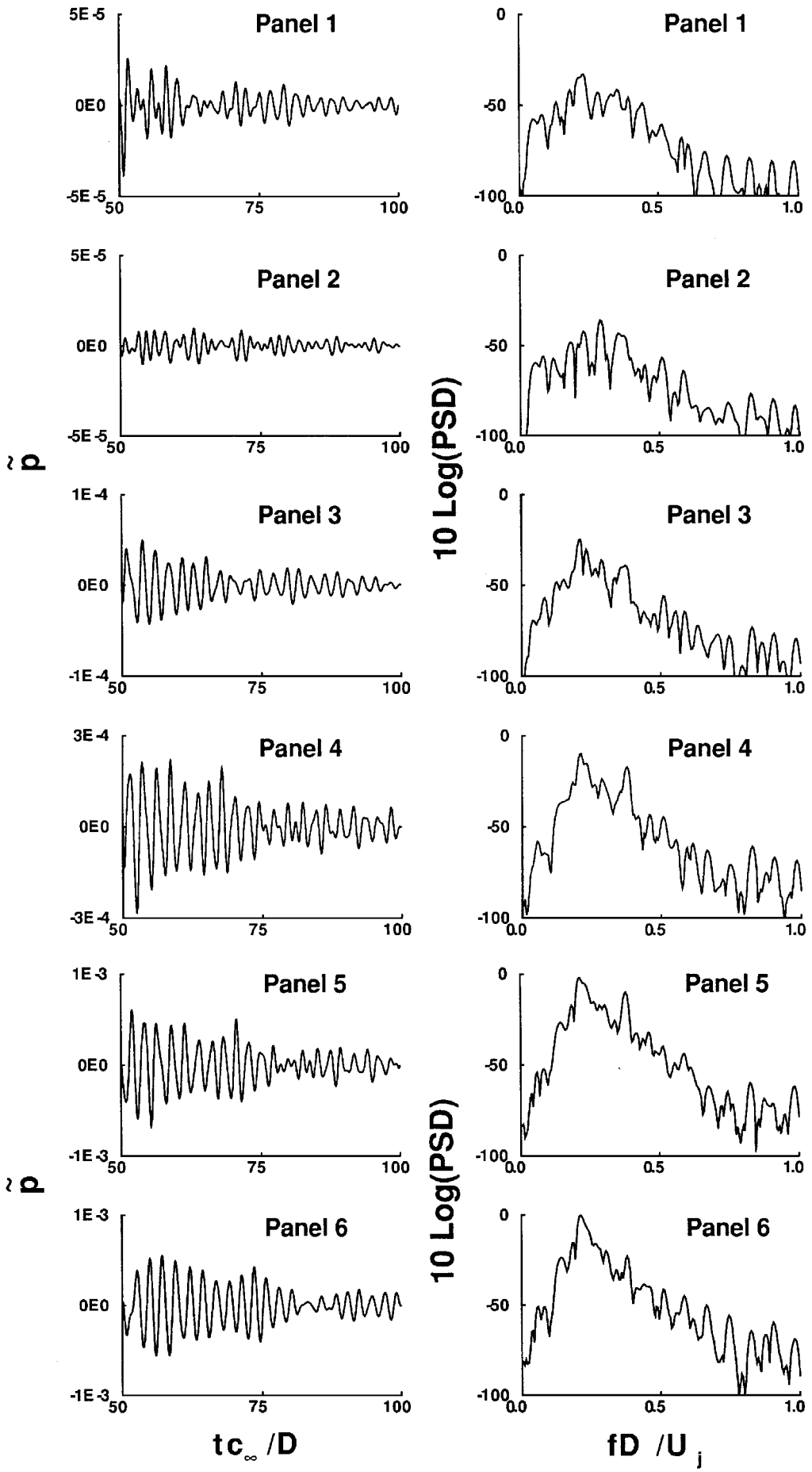

Fig. 9 $\tilde{p}$ **just below the panels at the panel centers.**

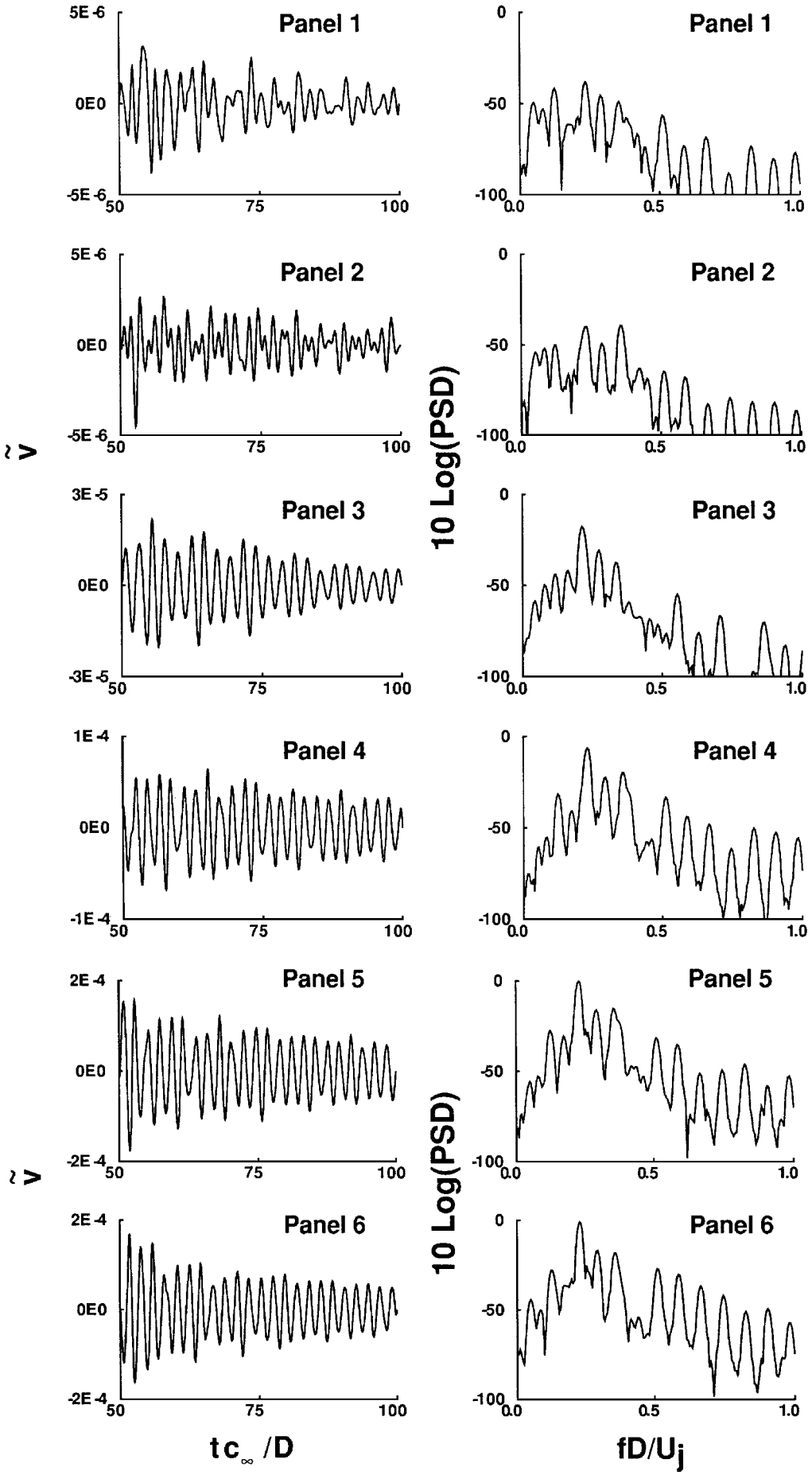

Fig. 10 $\tilde{v}$ at the panel centers.

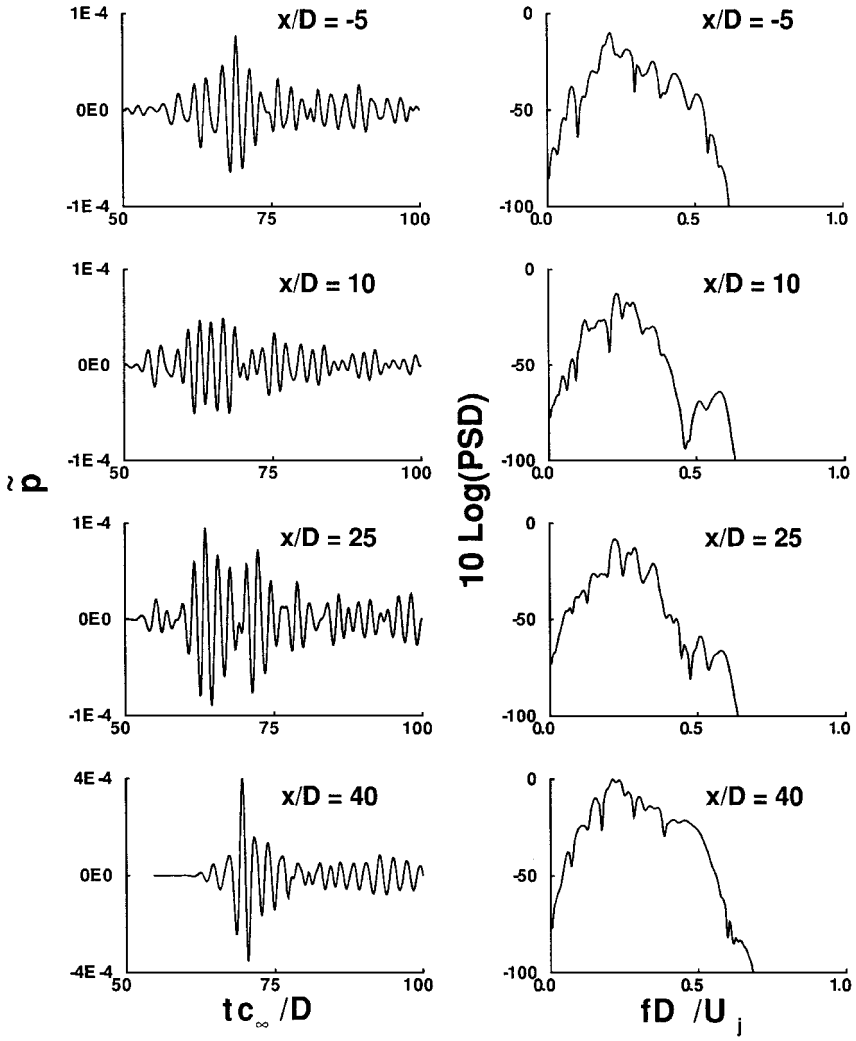

Fig. 11 $\tilde{p}$ **at four points along a line in the radiation domain.**

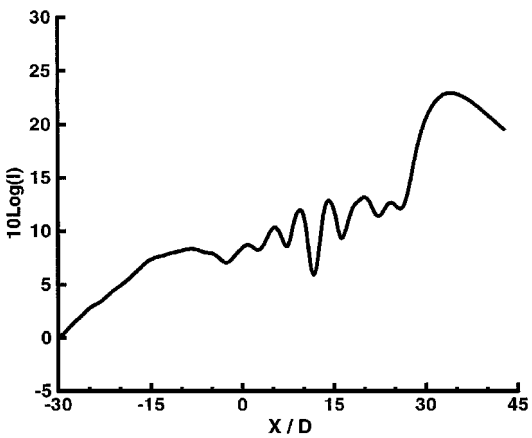

Fig. 12 Overall sound pressure level as a function of x **along a line in the radiation domain.**

the Mach angle for panels located within the Mach line relative to the jet. We note that this sensitivity would be expected to increase for a broader band incident field.

Finally, in Fig. 12, the overall sound pressure level is plotted as a function of x along this line. The figure shows the analog of the jet domain beaming in the radiation domain, consistent with Fig. 7. Again, the localized beaming of the radiated sound is in contrast to the behavior found for high subsonic jets.[3]

IV. Conclusions

We have computed the full unsteady fluid dynamic field, including the far-field acoustic pressure, in an excited supersonic jet. We have considered both a free jet and a jet that is installed near an array of flexible aircraft type panels. We have considered only the long time response of the jet/panel system. This response is dominated by a very pronounced and intense Mach wave radiation beam generated by a succession of cellular structures formed by convecting disturbances in the jet column. The long time pressure field in the jet has the following predominant features:

1) Pressure and velocity disturbances initiated near the nozzle lip give rise to a cellular structure within the jet. These cells expand and contract as they propagate downstream, generating acoustic waves that propagate into the far field at the Mach angle of the jet.

2) This Mach wave radiation is the most pronounced feature of the jet far field and is characterized by a peaked spectrum with a peak Strouhal number of approximately 0.21 (together with harmonics), close to observations for jets in this Mach number range. The peak frequency arises even though the jet is subject to transient (broadband) forcing. Thus there is a particular frequency, the jet frequency, associated with the long time response of the jet.

3) The acoustic pressure field for angles greater than the Mach angle is at a much lower level and appears to break up into irregular small-scale structures.

4) Near-field pressure is characterized by a relatively peaked spectrum near the jet exit and an increasingly continuous spectrum with increasing downstream distance.

5) Vortices associated with the pressure instability waves are significantly stretched as compared with lower Mach number jets.

We draw the following conclusions for the jet/flexible wall interaction:

1) The intense radiation of sound in the jet domain in the direction of the Mach angle observed in the free jet persists for the installed jet. However, the presence of the wall causes some distortion.

2) The loading of the panels depends crucially on location. Panels within the Mach line are subject to a high-level loading that peaks near the jet Strouhal number Sr_*. Panels upstream of the Mach line are subject to a low-level loading with a nearly continuous spectrum.

3) The panels within the Mach line exhibit a much larger response than panels outside of the Mach line, consistent with the $\tilde{p}$ just below the panels. The panel response is also peaked near the jet frequency.

4) The radiated pressure exhibits a beaming at roughly the same angle as in the jet domain. This radiated pressure emanates from panels excited by the jet Mach wave radiation. The pressure for points in this radiation beam exhibits a spectral peak close to the jet frequency. Therefore both the level and spectral content of interior sound are crucially dependent on location relative to panels within the Mach line.

Finally, we note that the results presented here are valid for the two-dimensional Cartesian jet that we considered in our computations. The extent to which these results are applicable to circular jets with axisymmetric or nonaxisymmetric disturbances remains to be determined.

Acknowledgments

The first author was supported by the NASA Langley Research Center while in residence under a National Research Council Postdoctoral Research Associateship Award. The second author was partially supported by the NASA Langley Research Center under Contract NAS1-19480 while in residence at the Institute for Computer Applications in Science and Engineering. The National Science Foundation provided additional support under Grants DMS 93-01635 and DMS 95-30937.

References

[1]McGreevy, J. L., Bayliss, A., and Maestrello, L., "Interaction of Jet Noise with a Nearby Panel Assembly," *AIAA Journal*, Vol. 33, No. 4, 1995, pp. 577–585.

[2]Bayliss, A., Maestrello, L., McGreevy, J. L., and Fenno, C. C., "Forward Motion Effects on Jet Noise, Panel Vibration, and Radiation," *AIAA Journal*, Vol. 34, No. 6, 1996, pp. 1103–1110.

[3]Fenno, C. C., Bayliss, A., and Maestrello, L., "Panel-Structure Response to Acoustic Forcing by a Nearly Sonic Jet," AIAA Paper 96-1762, 1996; also *AIAA Journal*, Vol. 35, No. 2, 1997, pp. 219–227.

[4]Lighthill, M. J., "On Sound Generated Aerodynamically-I, General Theory," *Proceedings of the Royal Society, Series A*, Vol. A222, 1954, pp. 1–32.

[5]Lilley, G. M., "Theory of Turbulence Generated Jet Noise: Generation of Sound in a Mixing Region," U.S. Air Force, AFAPL-TR-72-53, IV, Wright–Patterson AFB, OH, July 1972.

[6]Ribner, H. S., "Perspectives on Jet Noise," *AIAA Journal*, Vol. 19, No. 5, 1981, pp. 1513–1526.

[7]Ribner, H. S., "An Extension of the Lighthill Theory of Jet Noise to Encompass Refraction and Shielding," NASA TM-110163, May 1995.

[8]Ting, L., and Miksis, M. J., "On Vortical Flow and Sound Generation," *SIAM Journal on Applied Mathematics*, Vol. 50, No. 2, 1995, pp. 521–536.

[9]Ting, L., and Klein, R., *Viscous Vortical Flows*, No. 374, Lecture Notes in Physics, Springer–Verlag, Berlin, 1991.

[10]Crow, S., and Champagne, F., "Orderly Structure in Jet Turbulence," *Journal of Fluid Mechanics*, Vol. 48, 1971, pp. 457–591.

[11]Maestrello, L., Bayliss, A., and Turkel, E., "On the Interaction of a Sound Pulse with the Shear Layer of an Axisymmetric Jet," *Journal of Sound and Vibration*, Vol. 74, No. 2, 1981, pp. 281–301.

[12]Bechert, D. W., and Pfizenmaier, E., "On the Amplification of Broadband Jet Noise by Pure Tone Excitation," *Journal of Sound and Vibration*, Vol. 43, No. 3, 1975, pp. 581–587.

[13]Huerre, P., and Monkewitz, P. A., "Local and Global Instabilities in Spatially-Developing Flows," *Annual Review of Fluid Mechanics*, Vol. 22, 1990, pp. 473–537.

[14]Michalke, A., and Hermann, G., "On the Inviscid Instability of a Circular Jet with External Flow," *Journal of Fluid Mechanics*, Vol. 114, 1982, pp. 343–359.

[15]Michalke, A., "Survey on Jet Instability Theory," *Progress in Aerospace Science*, Vol. 21, No. 3, 1984, pp. 159–199.

[16]Bayliss, A., Maestrello, L., and Turkel, E., "On the Interaction of a Sound Pulse with the Shear Layer of an Axisymmetric Jet, III: Non-Linear Effects," *Journal of Sound and Vibration*, Vol. 107, No. 1, 1986, pp. 167–175.

[17]Maestrello, L., and Bayliss, A., "Flowfield and Far Field Acoustic Amplification Properties of Heated and Unheated Jets," *AIAA Journal*, Vol. 20, No. 11, 1982, pp. 1539–1546.

[18]Ffowcs Williams, J. E., and Kempton, A. J., "The Noise from the Large-Scale Structure of a Jet," *Journal of Fluid Mechanics*, Vol. 84, 1975, pp. 673–694.

[19]Seiner, J. M., "Fluid Dynamics and Noise Emission Associated with Supersonic Jets," *Studies in Turbulence*, edited by T. B. Gatski, S. Sarkar, and C. G. Speziale, Springer–Verlag, New York, 1992, pp. 297–323.

[20]Frendi, A., Maestrello, L., and Bayliss, A., "On the Coupling Between a Supersonic Boundary Layer and a Flexible Surface," *AIAA Journal*, Vol. 31, No. 4, 1993, pp. 708–713.

[21]Frendi, A., Maestrello, L., and Bayliss, A., "Coupling Between Plate Vibration and Acoustic Radiation," *Journal of Sound and Vibration*, Vol. 177, No. 2, 1994, pp. 207–226.

[22]Gottlieb, D., and Turkel, E., "Dissipative Two-Four Methods for Time-Dependent Problems," *Mathematics of Computation*, Vol. 30, 1976, pp. 703–723.

[23]Mankbadi, R., Hayder, M., and Povinelli, L., "The Structure of Supersonic Jet Flow and Its Radiated Sound," *AIAA Journal*, Vol. 32, 1994, pp. 897–906.

[24]McLaughlin, D. K., Morrison, G. L., and Trout, T. R., "Reynolds Number Dependence in Supersonic Jet Noise," *AIAA Journal*, Vol. 15, 1977, pp. 526–532.

S. Glegg
Associate Editor